Enhancement and suppression of mixing and diffusion in an axisymmetric jet by half delta-wing tabs

Y. Ito[a,*], K. Miura[b], Y. Sakai[a], K. Iwano[a]

[a]*Department of Mechanical Systems Engineering, Nagoya University, Furo-cho, Chikusa-ku, Nagoya, Aichi 464-8603, Japan*
[b]*Department of Mechanical Science and Engineering, Nagoya University, Furo-cho, Chikusa-ku, Nagoya, Aichi 464-8603, Japan*

Abstract

Effects of half delta-wing tabs on mixing and diffusion in an axisymmetric jet are experimentally investigated. The tabs are installed at the jet exit circumferentially with an equal interval. The number of the tab is varied from 1 to 6. The jet Reynolds number is set to 20,000. Instantaneous streamwise and radial (vertical or horizontal) velocities and temperature are mainly measured by a composite probe which consists of an X-type hot-wire and an I-type cold-wire. The results show that mixing with the ambient fluid is more enhanced with increasing the number of the tab near the jet exit. However, in the downstream region, it is suppressed in the cases with 4, 5, and 6 tabs and most suppressed in the case with 6 tabs, while it is most enhanced in the case with 3 tabs. The analysis based on the mean velocity distribution indicates that, although the spatially-averaged entrainment velocity is basically decreased by the tabs, the mixing and entrainment can be enhanced when the entrainment area is significantly increased. Thermal diffusion is more enhanced with increasing the number of the tab near the jet exit but, in the downstream region, it is equivalent or suppressed in the cases with the tabs. These results are caused by the mixed effects of the tabs: enhancement of not only mixing and diffusion but also the energy dissipation. The present study suggests that it is feasible to both promote and suppress mixing of the jet by the half delta-wing tabs, and directional characteristics of the jet diffusion can be controlled by optimizing the tab installation.

*Corresponding author

Email addresses: ito@nagoya-u.jp (Y. Ito), kmiura.nagoyau.mse@gmail.com (K. Miura), ysakai@mech.nagoya-u.ac.jp (Y. Sakai), iwano@nagoya-u.jp (K. Iwano)

Keywords: Turbulence, Jet control, Tabs, Diffusion, Entrainment, Mixing

1. Introduction

Jets with scalar transport are seen in a wide variety of industrial devices such as air conditioners, heat exchangers, jet engines, and combustors. Since the scalar transport is usually dominated by the flow field, flow control becomes of great importance to achieve the higher efficiency of the devices. Here flow control can be both enhancement and suppression of the diffusion and mixing. In some cases such as heat exchangers and jet engines, it is desired to enhance them. In other cases such as spot cooling, on the contrary, suppression of jet diffusion is desired to transport the scalar at a specific local point far from the jet exit.

Jet control methods can be categorized as active or passive, depending on requirement of external power source. A typical device based on the active control is an actuator installed in the jet nozzle [1–3]. The primary aim is to excite initial instability of the jet and enhance shedding of the vortex ring, which drastically changes the vortical structure of the jet.

On the other hand, passive control is usually based on modification of the geometry of the jet exit. The primary aim is to introduce streamwise vortices, which has cross-streamwise velocity components through reorientation of the vortex ring shed from the jet exit [4]. Typical examples are a non-circular nozzle [5, 6] and insertion of vortex-generating tabs at the jet exit [7–9]. As for the tabs, Zaman et al. [8] reported on the generation of the streamwise vorticity by delta and rectangular tabs in a subsonic axisymmetric jet. They showed that the source of the streamwise vorticity is the pressure gradient generated on the upstream side of the tab and the vortex filaments shed from the tab are reoriented by the mean velocity gradient. Nagata et al. [10] performed jet control using three types of tabs: delta tabs installed with angles of attack of 45 and 90 degrees, and a half delta-wing tab with an angle of attack of 30 degrees. They showed that the velocity fluctuation is generated between the tabs in the case of the delta tab with an angle of attack of 90 degrees, while it is generated behind the tabs in the case of 45 degrees and on the suction side in the case of the half delta-wing tab. They also showed that velocity field is modified more significantly in the case of the half delta-wing tabs. Regarding the effects of the angle of attack of the tabs, Carletti et al. [11] investigated the effects of a half delta-wing tab placed around the exit of an axisymmetric jet. They showed that the velocity distribution is symmetric against the tab when the angle of attack is 60 degrees, whereas it is asymmetric when the

angle of attack is 30 degrees. They also revealed that, when the angle of attack is less than 40 degrees, the half delta-wing tab produces single vortex, while the tab produces a pair of streamwise vortices when the angle of attack is larger than 40 degrees. Rogers and Parekh [12] also showed strong dependency of the angle of attack in a supersonic jet by flow visualization. Regarding the effects of the number of the tab, Bradbury and Khadem [7] investigated in an axisymmetric jet with 2, 4, and 8 square tabs. They found that the mean streamwise velocity near the jet exit in the case of 2 square tabs decreases most rapidly because the potential core splits into two parts. A similar result is reported by Mi and Nathan [13] in a slightly heated axisymmetric jet. They showed that, in the cases with 2 delta tabs, the mean temperature on the jet center decreases more rapidly and thermal diffusion far downstream from the jet exit is more enhanced compared to the 4 delta tabs case. Recent study [14] on a subsonic axisymmetric jet with 6 and 12 equally-arrayed triangular chevrons showed that the increase of azimuthal spacing between the adjacent chevrons reduces magnitude of the maximum streamwise vorticity near the jet nozzle and its decay becomes slower because the initial streamwise vortex interaction is reduced.

In the present study, we also applied half delta-wing tabs as vortex generators in an axisymmetric jet. It is aimed at clarifing the determining factor for jet control and finding the optimal conditions to maximize such effects.

2. Experiments

2.1. Experimental apparatus and conditions

Fig. 1(a) shows the schematic of the experimental apparatus. An axisymmetric air jet is generated by passing through a blower, a wind tunnel, and a round-shape skimmer. The skimmer has a diameter of $d = 30$ mm and its upstream side is sharpened to cut off boundary layer developed in the contraction section of the wind tunnel. An electric heater is installed at the air intake of the blower. The air temperature at the jet exit is monitored by a thermocouple and kept constant by a proportional-integral-differential (PID) heater controller. The initial velocity and temperature at the jet exit are kept constant. It is confirmed that the background velocity fluctuation at the jet exit relative to the initial jet velocity is less than 1% and the background temperature fluctuation relative to the temperature difference between the initial jet temperature and the ambient temperature is less than 0.5%. It is also confirmed that the temporal change of the ambient temperature during the experiment is negligibly small. The origin of the coordinates is set to the center of the jet exit and x, y, and z denote streamwise, vertical, and spanwise directions,

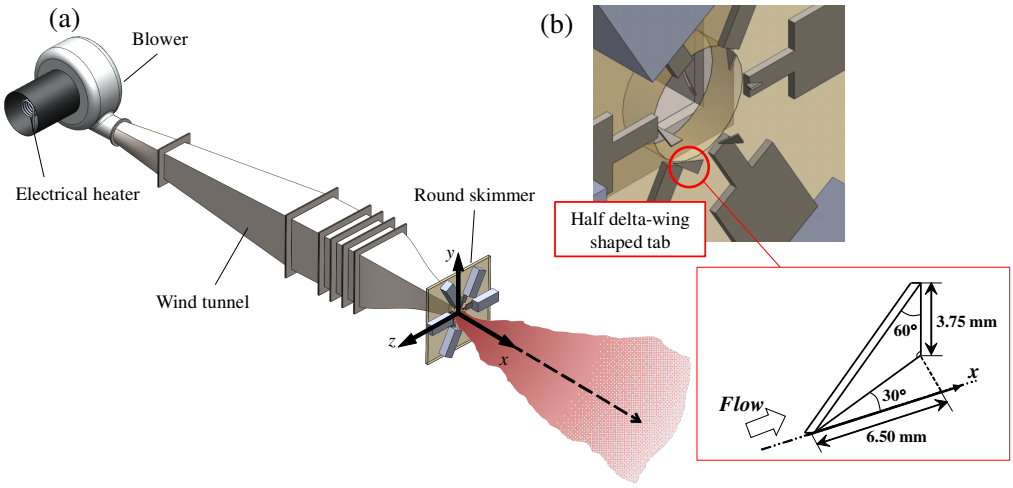

Figure 1: (a) Schematic of the experimental apparatus and (b) the tabs installed at the jet exit in the case with 6 tabs.

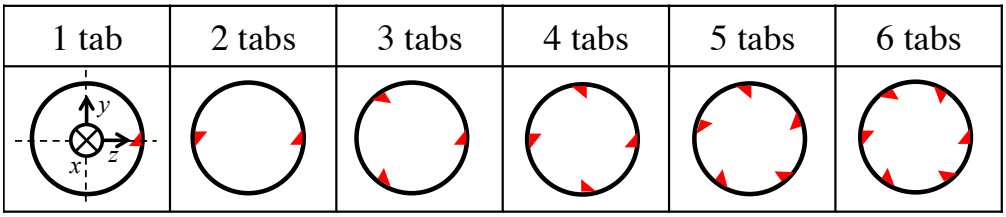

Figure 2: The arrangement of the tabs around the jet exit by the number of the tab.

respectively. In addition, radial direction r and azimuthal direction φ are defined as cylindrical coordinates.

Fig. 1(b) shows the tabs installed at the jet exit in the case with 6 tabs. Each tab has a half delta-wing shape and its height, length, and sweep angle are 3.75 mm, 6.50 mm, and 60 degrees, respectively. The tabs are arrayed around the jet exit with an equal interval (except in the case with 1 tab) as shown in Fig. 2. The angle of attack is set to 30 degrees. The solidity of single tab is 0.86%.

The Reynolds number based on the skimmer diameter d and the initial jet velocity U_J is set to $\mathrm{Re_J}(= U_J d/\nu) = 20{,}000$. Here, ν is the kinematic viscosity of the air. The fluid temperature at the jet exit Θ_J is set to 7.5 K higher than the ambient fluid temperature Θ_a. The Richardson number at the jet exit is $\mathrm{Ri_J}(= g\beta(\Theta_J - \Theta_a)d/U_j^2) \simeq 7.4 \times 10^{-5}$ where g and β are gravitational acceleration and

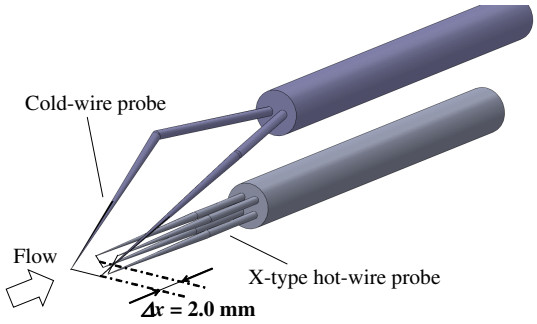

Figure 3: Schematic of the composite probe consisted of an X-type hot-wire probe and an I-type cold-wire probe.

cubical expansion coefficient, respectively. It is sufficiently small to regard heat as a passive scalar.

Instantaneous velocity and temperature are measured by a constant-temperature-type hot-wire anemometer and a constant-current-type cold-wire thermometer, respectively. The sensor part of the hot-wire anemometer and cold-wire thermometer consists of a fine tungsten wire. The diameter and length are 5 μm and 1 mm for the hot-wire and 3 μm and 2 mm for the cold-wire, respectively. Fig. 3 shows the schematic of the composite probe consisting of an X-type hot-wire probe and an I-type cold-wire probe used for simultaneous measurements of two velocities and temperature. The cold-wire is fixed 2.0 mm upstream from the hot-wire to minimize their interference. Note that non-composite probes are also used depending on the measurement situation.

The electronic signals from the hot-wire anemometer and cold-wire thermometer are converted to 16 bit digital signals by an A/D board (National Instruments PCIe-6343), and the data is stored in the computer (Dell Vostro 200). The sampling frequency is set to 20 kHz.

2.2. Compensations

Following compensations were applied to increase the measurement accuracy. Firstly, the compensation method proposed by Hirota et al. [15] is applied for velocity measurement when the flow has a large velocity gradient. For temperature measurement, gain decay and phase delay were compensated by the method proposed by Tagawa et al. [16]. Fig. 4(a) shows the power spectra for the temperature fluctuation at the jet center ($y/d = z/d = 0$) and $x/d = 9.0$ in the cases with and without the frequency compensation. It confirms that the power spectrum in the

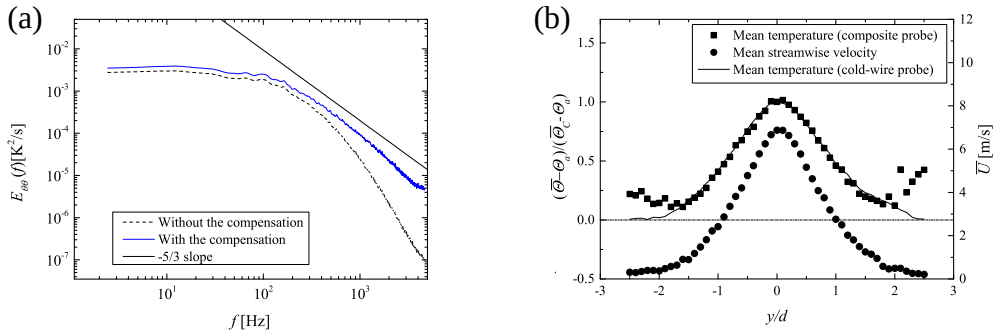

Figure 4: Comparison of the data before and after the compensation. (a) Power spectra for the temperature fluctuation at the jet center and x/d = 9.0 in the cases without and with the frequency compensation; (b) transverse profile of the mean temperature and mean streamwise velocity at x/d = 9.0.

case with the compensation is larger than that in the case without the compensation and the inertial subrange region following -5/3 power law becomes clearer. Finally, in the simultaneous measurements for velocity and temperature, thermal compensation proposed by Brunn [17] is applied. The output voltage E_a from the hot-wire probe is corrected by

$$E_{a,r} = E_a\left(\frac{\Theta_w - \Theta_r}{\Theta_w - \Theta_a}\right)^{1/2}, \tag{1}$$

where $E_{a,r}$ is the compensated voltage, Θ_w is the wire's temperature, and Θ_r is the reference temperature. In addition, the spatial gap between the hot-wire and cold-wire probes Δx was compensated using the Taylor's frozen hypothesis;

$$\Delta t = \frac{\Delta x}{\overline{U}}, \tag{2}$$

where Δt and $\overline{U}$ denote the temporal delay and mean streamwise velocity, respectively. Both of the two corrections in Eqs. (1) and (2) are digitally processed after the data acquisition. Fig. 4(b) shows the transverse profiles of the mean temperature at x/d = 9.0 measured by the composite probe and only the cold-wire probe. The two data are mostly identical except at the outer region of the jet, proving that the thermal influence generated by the hot-wire is negligible except the low-speed regions.

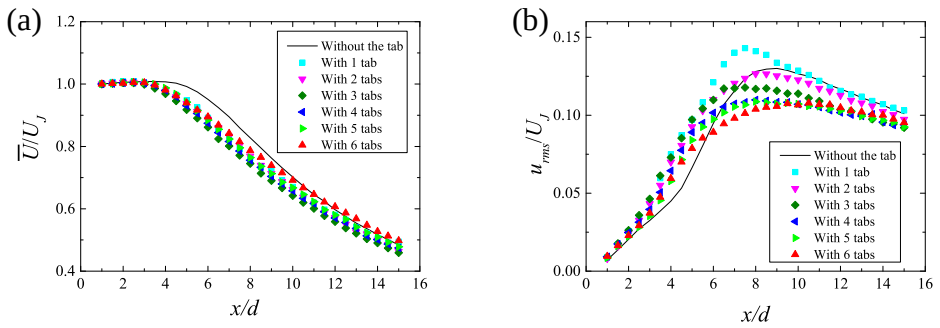

Figure 5: Streamwise profiles of (a) the normalized mean streamwise velocity and (b) the normalized streamwise rms velocity at the jet center.

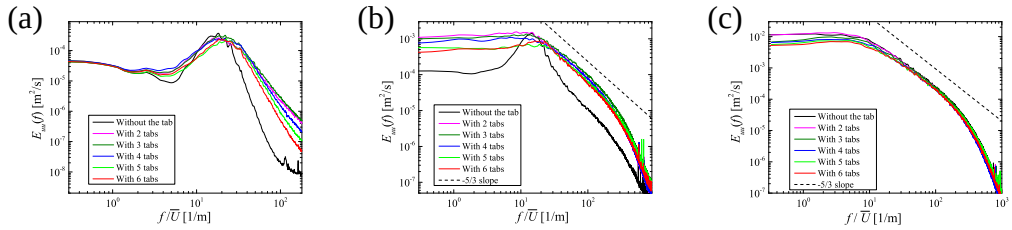

Figure 6: Power spectra for the streamwise velocity fluctuation at the jet center and (a) $x/d = 2.0$, (b) $x/d = 4.0$, and (c) $x/d = 9.0$.

3. Results and Discussion

3.1. Velocity field

Fig. 5 shows the streamwise profiles of (a) the normalized mean streamwise velocity $\overline{U}/U_J$ and (b) the normalized streamwise rms velocity u_{rms}/U_J at the jet center ($y/d = z/d = 0$) in the cases without the tab and with 1–6 tabs. Fig. 5(a) reveals that $\overline{U}/U_J$ starts to decrease earlier and the potential core becomes shorter in the cases with the tabs. As the flow goes in the downstream direction, $\overline{U}/U_J$ in the cases with 1–6 tabs approaches that in the case without the tab. $\overline{U}/U_J$ in the case with 6 tabs becomes larger than that in the case without the tab at $x/d = 15$, while $\overline{U}/U_J$ in the cases with 2–5 tabs is still smaller. On the other hand, Fig. 5(b) illustrates that the tabs increase u_{rms}/U_J near the jet exit and the peak in the cases with 1–4 tabs appears earlier than that in the case without the tab. However, the peak values in the cases with 2–6 tabs are smaller than that in the case without the tab. Note that, as shown later, the jet center is shifted in the case with 1 tab so we will exclude this case from the present discussion. In the downstream region,

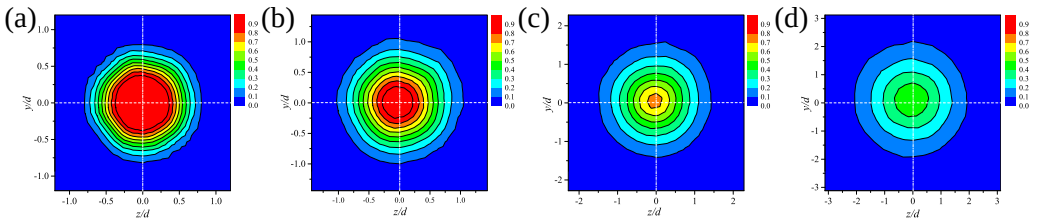

Figure 7: Contour maps of the normalized mean streamwise velocity in the case without the tab at (a) $x/d = 2.0$, (b) $x/d = 4.0$, (c) $x/d = 9.0$, and (d) $x/d = 15.0$.

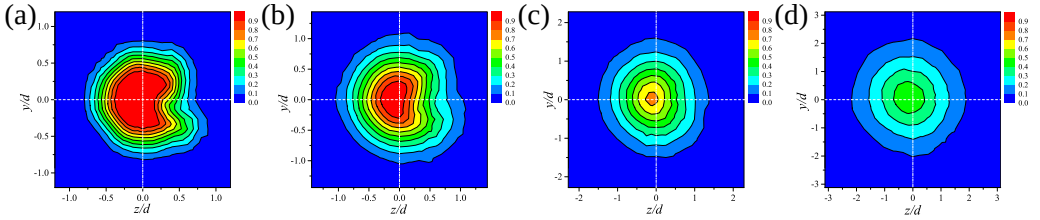

Figure 8: Contour maps of the normalized mean streamwise velocity in the case with 1 tab at (a) $x/d = 2.0$, (b) $x/d = 4.0$, (c) $x/d = 9.0$, and (d) $x/d = 15.0$.

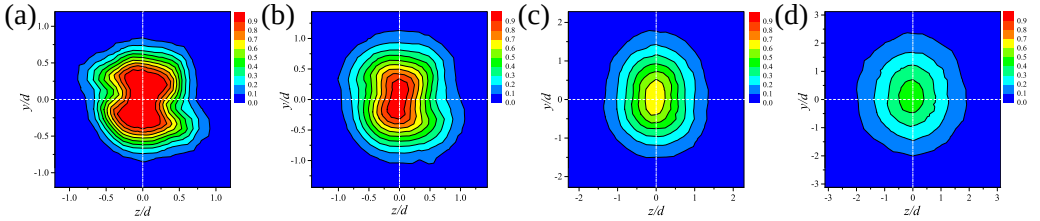

Figure 9: Contour maps of the normalized mean streamwise velocity in the case with 2 tabs at (a) $x/d = 2.0$, (b) $x/d = 4.0$, (c) $x/d = 9.0$, and (d) $x/d = 15.0$.

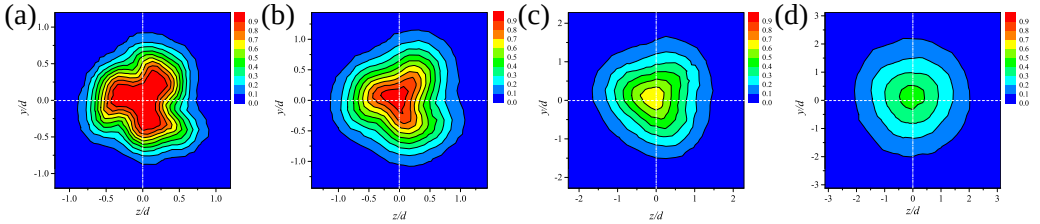

Figure 10: Contour maps of the normalized mean streamwise velocity in the case with 3 tabs at (a) $x/d = 2.0$, (b) $x/d = 4.0$, (c) $x/d = 9.0$, and (d) $x/d = 15.0$.

u_{rms}/U_J in the cases with the tabs is smaller than that in the case without the tab, meaning that the turbulence intensity is smaller.

Fig. 6 shows the power spectra for the streamwise velocity fluctuation $E_{uu}(f)$

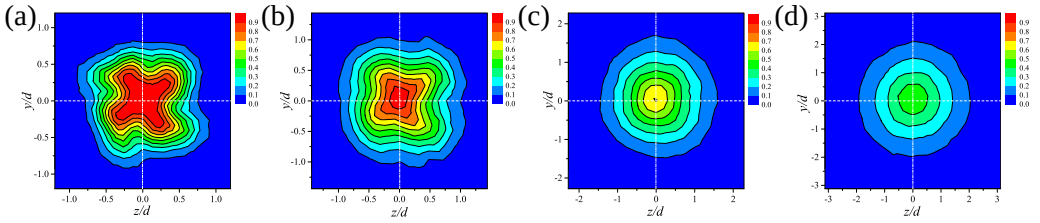

Figure 11: Contour maps of the normalized mean streamwise velocity in the case with 4 tabs at (a) $x/d = 2.0$, (b) $x/d = 4.0$, (c) $x/d = 9.0$, and (d) $x/d = 15.0$.

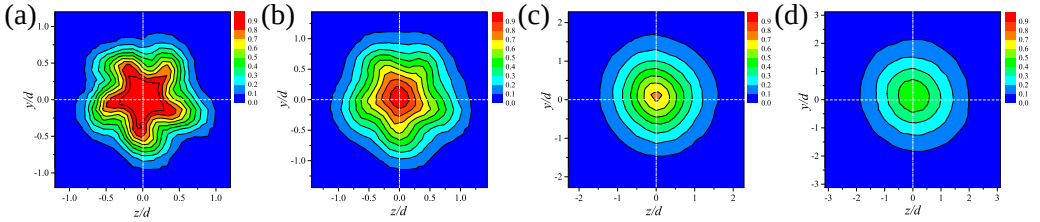

Figure 12: Contour maps of the normalized mean streamwise velocity in the case with 5 tabs at (a) $x/d = 2.0$, (b) $x/d = 4.0$, (c) $x/d = 9.0$, and (d) $x/d = 15.0$.

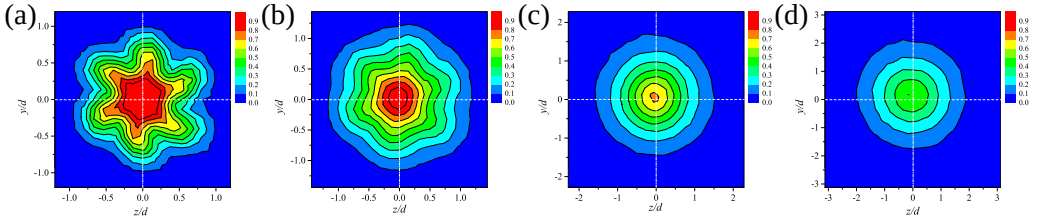

Figure 13: Contour maps of the normalized mean streamwise velocity in the case with 6 tabs at (a) $x/d = 2.0$, (b) $x/d = 4.0$, (c) $x/d = 9.0$, and (d) $x/d = 15.0$.

in the cases without the tab and with 2–6 tabs at the jet center and $x/d = 2.0$, 4.0, and 9.0. The horizontal axis is the frequency normalized by the mean streamwise velocity. At $x/d = 2.0$, a peak appears at around $f/\overline{U} = 20$ in all cases. This is caused by the initial instability at the jet exit. Note that the slope in the region of $f/\overline{U} > 20$ is more gentle in the cases with the tabs. At $x/d = 4.0$, the peak disappears and the inertial subrange that follows the -5/3 law appears in the cases with the tabs, whereas the peak still remains and the slope is still steep in the case without the tab. At $x/d = 9.0$, the jet in all cases becomes turbulence with the inertial subrange.

Figs. 7–13 show the contour maps of the normalized mean streamwise velocity $\overline{U}/U_J$ at $x/d = 2.0$, 4.0, 9.0, and 15.0 in the cases without the tab and with 1–6 tabs, respectively. In the upstream region, the cross-sectional shape of the jet is

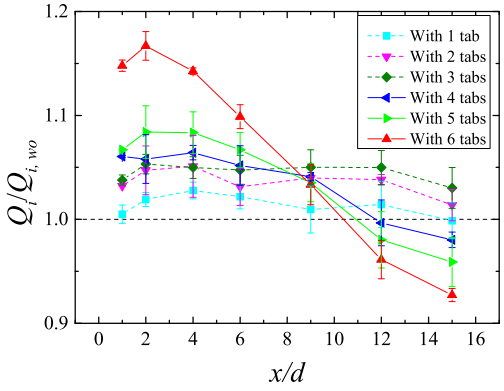

Figure 14: Streamwise profiles of the ratio of the mean flow rate between with and without the tabs cases.

distorted according to the tab configuration. As the flow goes in the downstream direction, the contours approach round though it is still oval at $x/d = 15$ in the case with 2 tabs. This tendency is similar to the case with 2 delta tabs in the past study [13]. In the case with 1 tab, jet center is shifted to the opposite side from the tab.

The mean flow rate Q was calculated by integrating the mean streamwise velocity on the y–z plane. Fig. 14 shows the streamwise profiles of the ratio of the mean flow rate between with and without the tabs cases. Here, Q_i is the mean flow rate at $x/d = i$ and wo denotes the value in the case without the tab. The integration area is taken sufficiently large that includes the area of $\overline{U}/U_J \simeq 0$. In the upstream region, $Q_i/Q_{i,wo}$ becomes large with increasing the number of the tab, meaning that mixing with the ambient fluid is enhanced according to the number of the tab. However, as the flow goes in the downstream direction, the mixing effect becomes weak, and at $x/d = 15$, the mean flow rate in the cases with 4–6 tabs is smaller than that in the case without the tab. The difference is most significant in the case with 6 tabs. On the other hand, the mean flow rate in the cases with 1–3 tabs keeps larger than that in the case without the tab in the measured region. In particular, it is the largest in the case with 3 tabs. Since the cases with 3 and 6 tabs show the most significant changes, these two cases will be mainly discussed in the following sections.

The mean entrainment rate of the ambient fluid per unit streamwise length q_e

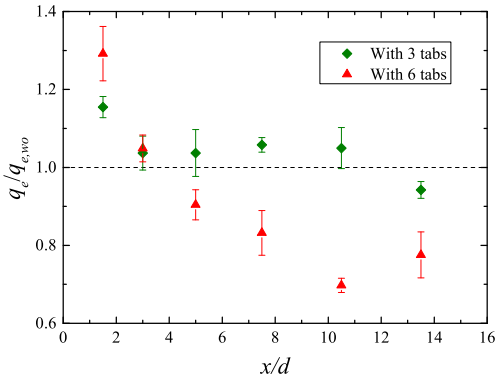

Figure 15: Streamwise profiles of the ratio of the mean entrainment rate between with and without the tabs cases.

can be calculated as follows:

$$q_e = \frac{Q_j - Q_i}{(j-i)d}, \tag{3}$$

where $j > i$. Fig. 15 shows the ratio of the mean entrainment rate between with and without the tabs cases $q_e/q_{e,wo}$. Since the cross-sectional measurements were carried out at x/d = 1, 2, 4, 6, 9, 12, and 15, q_e was obtained at x/d = 1.5, 3, 4.5, 7.5, 10.5, and 13.5. In $x/d < 4$, q_e in the cases with 3 and 6 tabs is larger than that in the case without the tab. However, in the downstream region, q_e in the case with 6 tabs becomes smaller compared to that in the case without the tab while that in the case with 3 tabs is slightly larger until x/d = 12.

q_e at a fixed streamwise location can be defined by

$$q_e = \int V_e dl, \tag{4}$$

where V_e is the local entrainment velocity and l is the integral route along the line that V_e is defined, typically at the turbulent/non-turbulent interface [18]. However, it is impossible to determine V_e and l in the present experiments. Therefore, we assumed that V_e can be represented by the mean velocity gradient normal to the isopleth of the half width for the mean velocity $\frac{d\overline{U}}{dn}$, where n is the coordinate axis normal to the isopleth and directs outward of the jet, because the mean velocity gradient is the original driving force of the fluid motion. For the interfacial area,

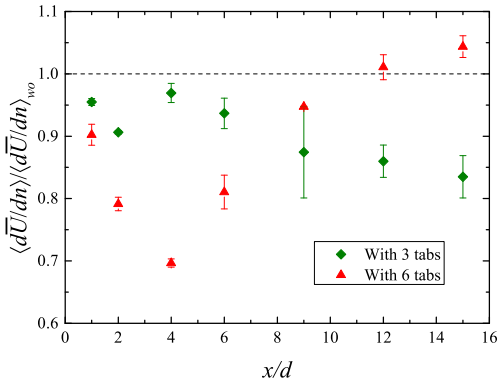

Figure 16: Streamwise profiles of the ratio of the spatially-averaged mean velocity gradient along the isopleth of the half width for the mean velocity between with and without the tabs cases.

we assumed that it can be represented by the isopleth length of the half width for the mean velocity L,

$$L = \int_{\overline{U}/U_C=0.5} dl. \tag{5}$$

Obviously U_C is the mean velocity at the jet center and l is taken along the isopleth. Fig. 16 show the ratio of the spatially-averaged $d\overline{U}/dn$ between with and without the tabs cases. In the figure, $\langle\ \rangle$ means the spatially-averaged value on the y–z plane. Interestingly, $\langle\frac{d\overline{U}}{dn}\rangle$ is generally smaller in both cases with 3 and 6 tabs than that in the case without the tab. This fact indicates that the averaged entrainment velocity is ought be smaller in the cases with the tabs. On the other hand, Figs. 17 (a) and (b) respectively show the streamwise profiles of L and its ratio between with and without the tabs cases. It is illustrated that the entrainment area is larger in the entire region in the case with 3 tabs whereas it is larger only in $x/d < 6$ in the case with 6 tabs. In summary, the mean entrainment rate can be determined by the balance of the entrainment velocity (represented by the mean velocity gradient at the half width for the mean velocity) and the entrainment area (represented by the isopleth length of $\overline{U}/U_C = 0.5$). Though the spatially-averaged mean velocity gradient is decreased by installing the tabs, when the entrainment area is significantly increased, mixing with the ambient fluid is enhanced.

To investigate the changes in the entrainment area in detail, Fig. 18 shows the

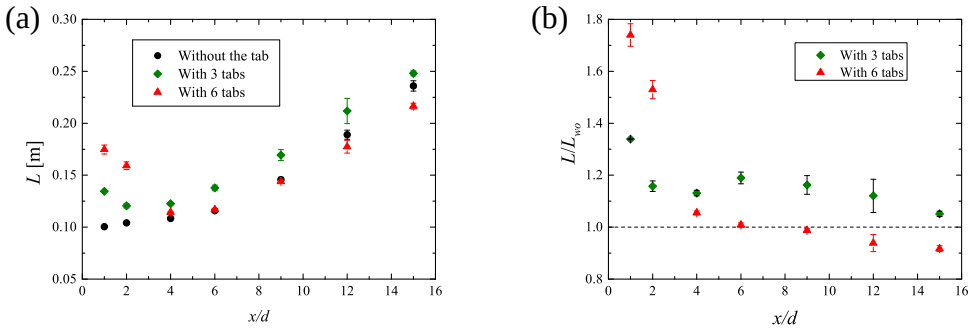

Figure 17: Streamwise profiles of (a) the isopleth length of the half width for the mean velocity and (b) its ratio between with and without the tabs cases.

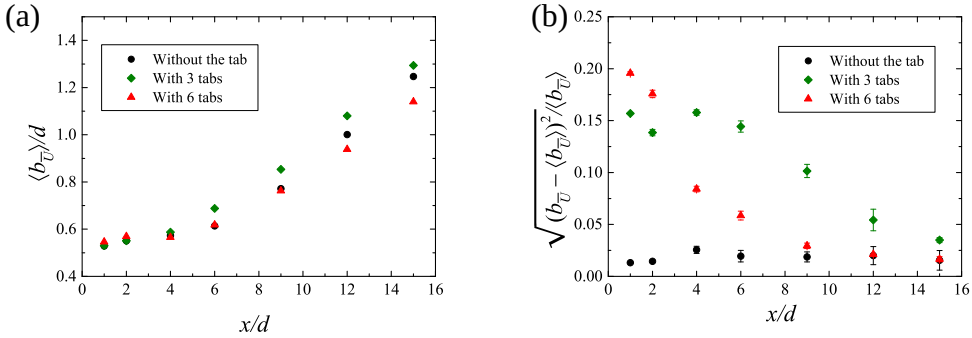

Figure 18: Streamwise profiles of (a) the spatially-averaged half width of the mean velocity normalized by the skimmer diameter and (b) its spatial variance normalized by the half width.

streamwise profiles of (a) the spatially-averaged half width of the mean velocity normalized by the skimmer diameter $\langle b_{\overline{U}} \rangle / d$ and (b) its spatial standard deviation normalized by the averaged half width $\sqrt{(b_{\overline{U}} - \langle b_{\overline{U}} \rangle)^2} / \langle b_{\overline{U}} \rangle$. Comparison of Figs. 17(a) and 18(a) confirms that the distortion of $\overline{U}$ causes larger L in $x/d < 4$ in the cases with tabs. It is also found that, in this region, $\langle b_{\overline{U}} \rangle / d$ is almost constant and the same as that in the case with out the tab despite that L decreases in the streamwise direction in the cases with 3 and 6 tabs. This means that the distorted mean velocity profile on the y–z plane is smoothened without spreading out the jet in the radial direction. $\langle b_{\overline{U}} \rangle / d$ starts to increase from $x/d = 4$ but it is smaller in the case with 6 tabs than that in the case without the tab. In addition, the spatial standard deviation decreases significantly (Fig. 18(b)). As a result, L in the case with 6 tabs becomes smaller than that in the case without the tab in the downstream

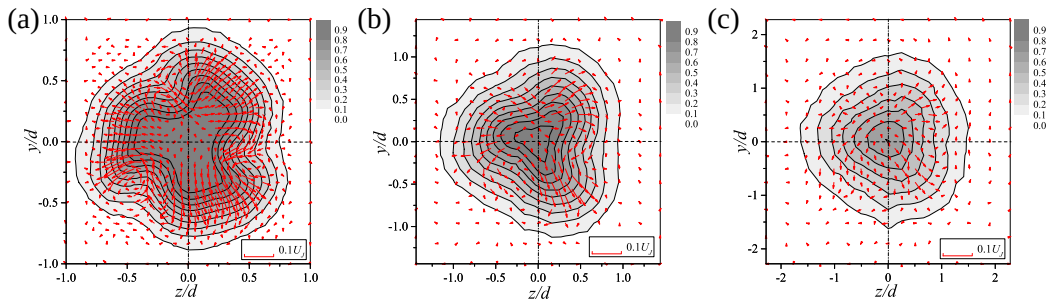

Figure 19: Normalized mean cross-streamwise velocity vector superposed on the contour maps of the mean streamwise velocity in the case with 3 tabs at (a) $x/d = 2.0$, (b) $x/d = 4.0$, and (c) $x/d = 9.0$.

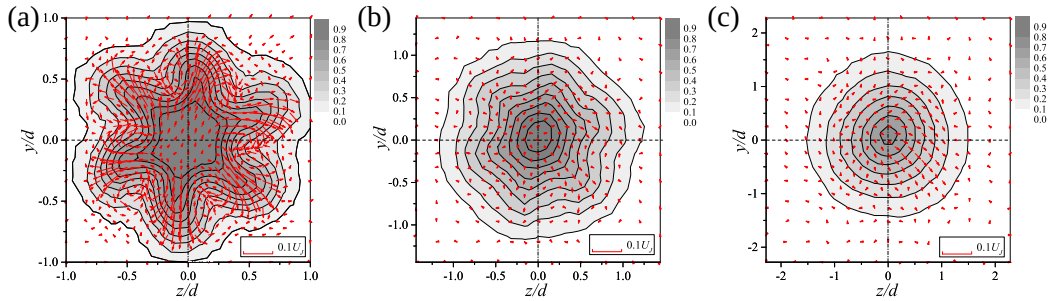

Figure 20: Normalized mean cross-streamwise velocity vector superposed on the contour maps of the mean streamwise velocity in the case with 6 tabs at (a) $x/d = 2.0$, (b) $x/d = 4.0$, and (c) $x/d = 9.0$.

region. On the other hand, both $\langle b_{\overline{U}} \rangle / d$ and its spatial standard deviation are larger in the case with 3 tabs, which results in larger L compared with the case without the tab.

Figs. 19 and 20 show the normalized mean cross-streamwise velocity vector superposed on the contour maps of the mean streamwise velocity at $x/d = 2.0$, 4.0, and 9.0 in the cases with 3 and 6 tabs, respectively. Here, the vector length reflects the mean cross-streamwise velocity $\sqrt{\overline{V}^2 + \overline{W}^2}/U_J$, where $\overline{V}$ and $\overline{W}$ are the mean vertical and spanwise velocities, respectively. Each tab is supposed to generate a deflected flow on the upstream side of the tab and a streamwise vortex, which should appear as a strong clockwise flow, on the downstream side. However, even at $x/d = 2.0$, these flows are not observed independently in either case. Instead, a simple flow pattern that the jet spreads out from between the tabs and recirculates back to the center at behind the tabs is observed in both cases with 3 and 6 tabs. As the flow goes in the downstream direction and the streamwise

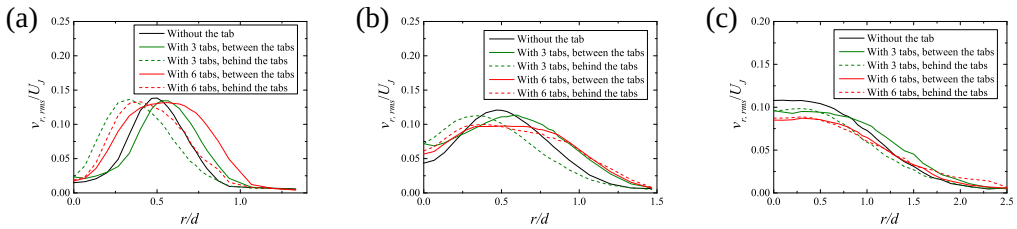

Figure 21: Radial profiles of the normalized radial rms velocity at (a) $x/d = 2.0$, (b) $x/d = 4.0$, and (c) $x/d = 9.0$.

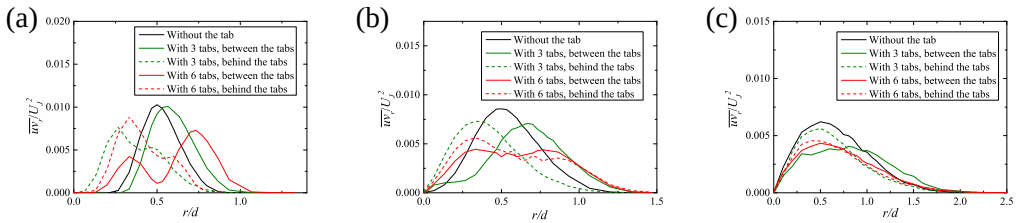

Figure 22: Radial profiles of the normalized Reynolds shear stress at (a) $x/d = 2.0$, (b) $x/d = 4.0$, and (c) $x/d = 9.0$.

velocity profiles approach round, such a flow pattern gradually merge and disappear though it weakly remains in the case with 3 tabs. Similar trend for vorticity is reported by Heeb et al. [14].

Fig. 21 shows the radial profile of the normalized radial rms velocity $v_{r,rms}/U_J$ at $x/d = 2.0$, 4.0, and 9.0. Note that the characteristics depend on the azimuthal location in the cases with the tabs. In addition, the measurable data is limited. Thus we show the profiles along the y– and z–axes, which correspond to either between the tabs or behind the tabs, depending on the configuration. At $x/d = 2.0$, the maximum value of $v_{r,rms}/U_J$ in the cases with 3 and 6 tabs is almost the same as that in the case without the tab. At behind the tabs, the peak shifts to the inner side, particularly in the case with 3 tabs, while the peak between the tabs shifts to the outside. However, $v_{r,rms}/U_J$ on both inner and outer sides becomes large in the case with 6 tabs while only that on the outer side becomes large in the case with 3 tabs, with respect to the case without the tab. At $x/d = 4.0$, the profiles are similar to those at $x/d = 2.0$ in the cases without the tab and with 3 tabs. On the other hand, in the case with 6 tabs, the profiles between the tabs and behind the tab are almost the same and the peak value is smaller than that in the other cases, although they are still larger in the central and outer regions in comparison with the case without the tab. At $x/d = 9.0$, the peak appears at the jet center, and among the

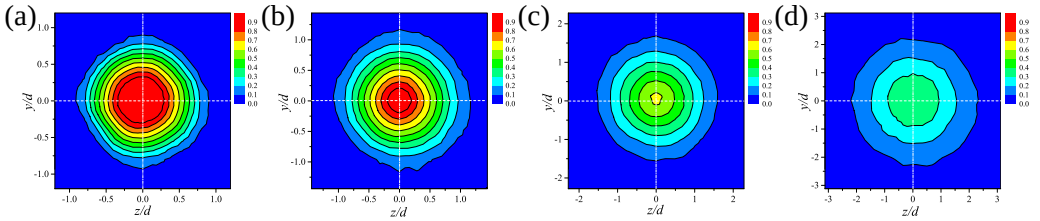

Figure 23: Contour maps of the normalized mean temperature in the case without the tab at (a) x/d = 2.0, (b) x/d = 4.0, (c) x/d = 9.0, and (d) x/d = 15.0.

three cases, that in the case without the tab is the largest. Furthermore, $v_{r,rms}/U_J$ in the case with 6 tabs is smaller in the entire region. As shown in Fig. 6, the tabs accelerate transition to turbulence and increase the small-scale disturbances as well as jet diffusion. However, from an energy point of view, this basically leads to the promotion of energy dissipation since the lifetime of a turbulent eddy is a function of l_e^2/ν, where l_e is the eddy size. Therefore, in the downstream region, the turbulence energy becomes smaller in the cases with the tabs, which causes the suppression of entrainment and mixing.

The same profiles for the normalized Reynolds shear stress $\overline{uv_r}/U_j^2$ is shown in Fig. 22. It illustrates that their general profiles are similar to those of $v_{r,rms}/U_J$ and the discussion above is confirmed. The decrease of $\overline{uv_r}/U_j^2$ appearing at r/d = 0.5 between the tabs in the case with 6 tabs at x/d = 2.0 is caused by the flat profiles of the mean streamwise velocity [9, 19].

3.2. Thermal field

Figs. 23–29 show the contour maps of the normalized mean temperature $(\overline{\Theta} - \Theta_a)/(\Theta_J - \Theta_a)$ on the y–z plane at x/d = 2.0, 4.0, 9.0, and 15.0 in the cases without the tab and with 1–6 tabs, respectively. The overall profiles are similar to the mean streamwise velocity profiles. The tabs distort the mean temperature profile near the exit but the profile becomes round in the downstream region. The tendency appears more clearly with increasing the number of the tab.

To quantitatively evaluate the effects of the tabs on thermal diffusion, entropy S based on the mean temperature on the y–z plane was calculated. Here S is defined as following based on the Boltzmann's law [20],

$$S \simeq \underbrace{k\Phi \ln \Phi}_{S_{sta}} \underbrace{-k \iint \phi \ln \phi dydz}_{S_{flu}}, \tag{6}$$

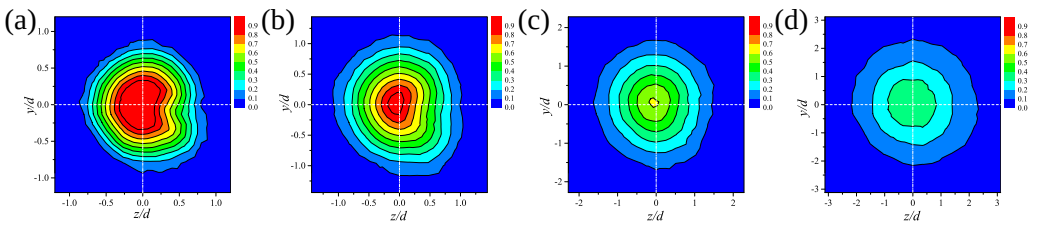

Figure 24: Contour maps of the normalized mean temperature in the case with 1 tab at (a) x/d = 2.0, (b) x/d = 4.0, (c) x/d = 9.0, and (d) x/d = 15.0.

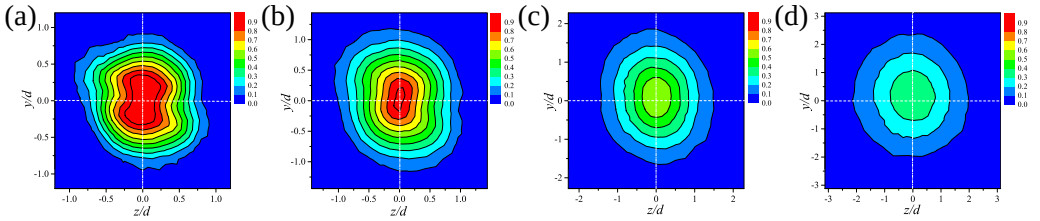

Figure 25: Contour maps of the normalized mean temperature in the case with 2 tabs at (a) x/d = 2.0, (b) x/d = 4.0, (c) x/d = 9.0, and (d) x/d = 15.0.

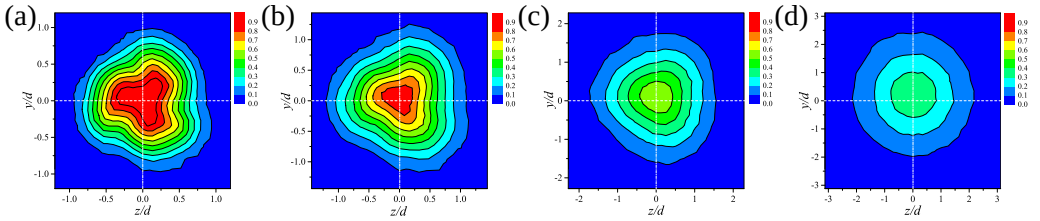

Figure 26: Contour maps of the normalized mean temperature in the case with 3 tabs at (a) x/d = 2.0, (b) x/d = 4.0, (c) x/d = 9.0, and (d) x/d = 15.0.

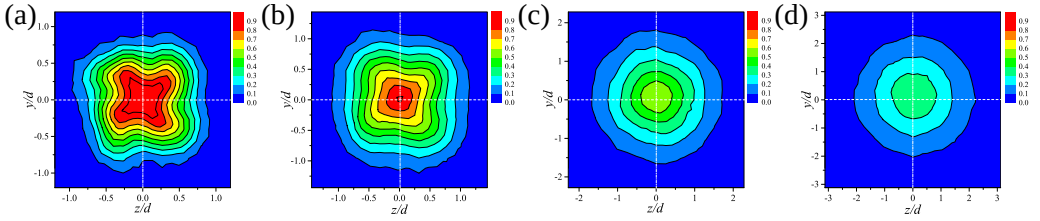

Figure 27: Contour maps of the normalized mean temperature in the case with 4 tabs at (a) x/d = 2.0, (b) x/d = 4.0, (c) x/d = 9.0, and (d) x/d = 15.0.

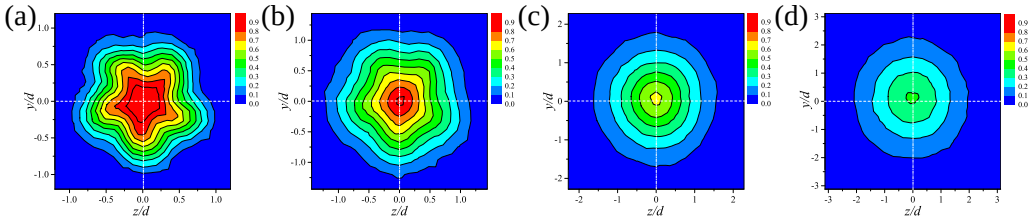

Figure 28: Contour maps of the normalized mean temperature in the case with 5 tabs at (a) x/d = 2.0, (b) x/d = 4.0, (c) x/d = 9.0, and (d) x/d = 15.0.

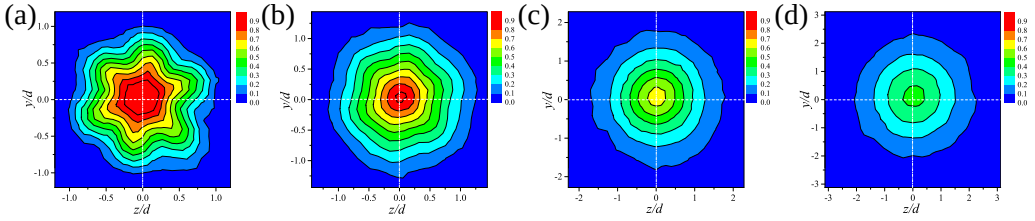

Figure 29: Contour maps of the normalized mean temperature in the case with 6 tabs at (a) x/d = 2.0, (b) x/d = 4.0, (c) x/d = 9.0, and (d) x/d = 15.0.

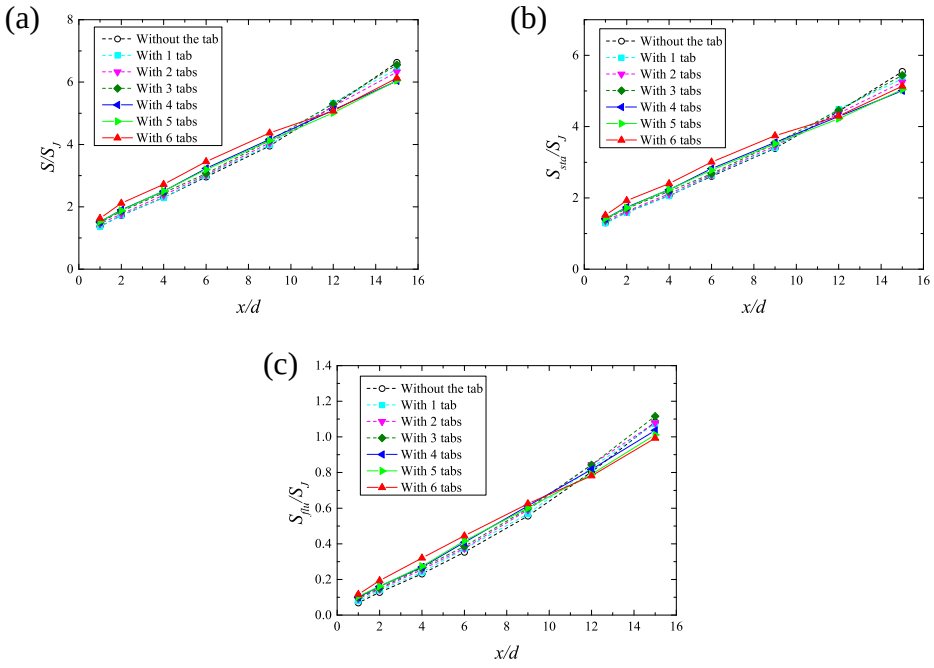

Figure 30: Streamwise profiles of the normalized (a) entropy, (b) statistical entropy, and (c) fluctuation entropy.

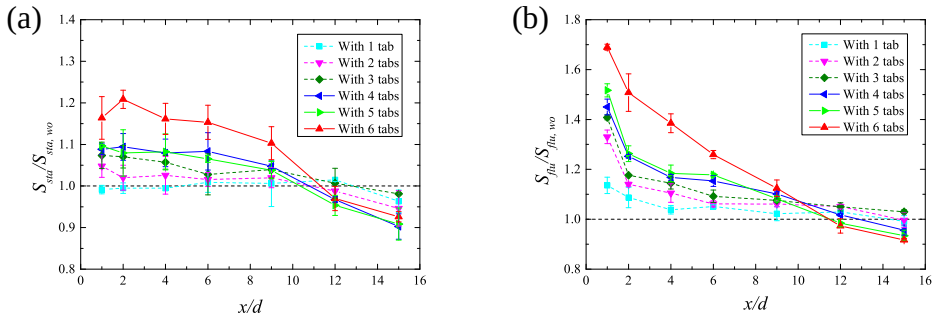

Figure 31: Streamwise profiles of (a) the ratio of the statistical entropy and (b) the ratio of the fluctuation entropy between the cases with and without the tabs.

where k is the Boltzmann constant and assumed as $k = 1$ in the present study, ϕ is the normalized mean temperature $\phi = (\overline{\Theta} - \Theta_a)/(\Theta_J - \Theta_a)$, and Φ is surface integral of ϕ: $\Phi = \iint \phi dydz$. As shown in Eq. (6), S is composed by two terms, S_{sta} and S_{flu}. The first term is called as the statistical entropy and, in the present case, the cross-sectional summation of the normalized local temperature at each streamwise location. On the other hand, the second term is called as the fluctuation entropy and denotes turbulent scalar diffusion. Fig. 30 shows the streamwise profiles of the normalized entropy and its breakdown. Here, S_J is the entropy at the jet exit. Also Fig. 31 shows (a) $S_{sta}/S_{sta,wo}$ and (b) $S_{flu}/S_{flu,wo}$. It is found that S is mainly determined by S_{sta} and basically increases with the number of the tab in the upstream region, but the magnitude order is reversed in the downstream region. This is the product of the mixed effects of the tabs: enhancement of not only mixing and diffusion but also the energy dissipation. On the contrary, the profile of S_{flu} is very similar to that of the mean flow rate and that in the case with 3 tabs is larger than that in the case without the tab even in the downstream region, where S_{sta} in the case with 3 tabs is smaller than that in the case without the tab. Therefore, it can be said that turbulent diffusion is most enhanced in the case with 3 tabs, as well as the entrainment and mixing.

To discuss the similarity of the momentum and thermal diffusion, turbulent Prandtl number $\mathrm{Pr_T}$ was calculated at the half width of the mean velocity,

$$\mathrm{Pr_T} = \frac{\nu_T}{\alpha_T} = \left.\frac{-\overline{uv_r}/(d\overline{U}/dr)}{-\overline{v_r\theta}/(d\overline{\Theta}/dr)}\right|_{\overline{U}/U_C=0.5}. \tag{7}$$

Here, ν_T and α_T are the eddy diffusivity coefficient and turbulent heat diffusivity coefficient, respectively. Fig. 32(a) shows the streamwise profiles of $\mathrm{Pr_T}$ in the

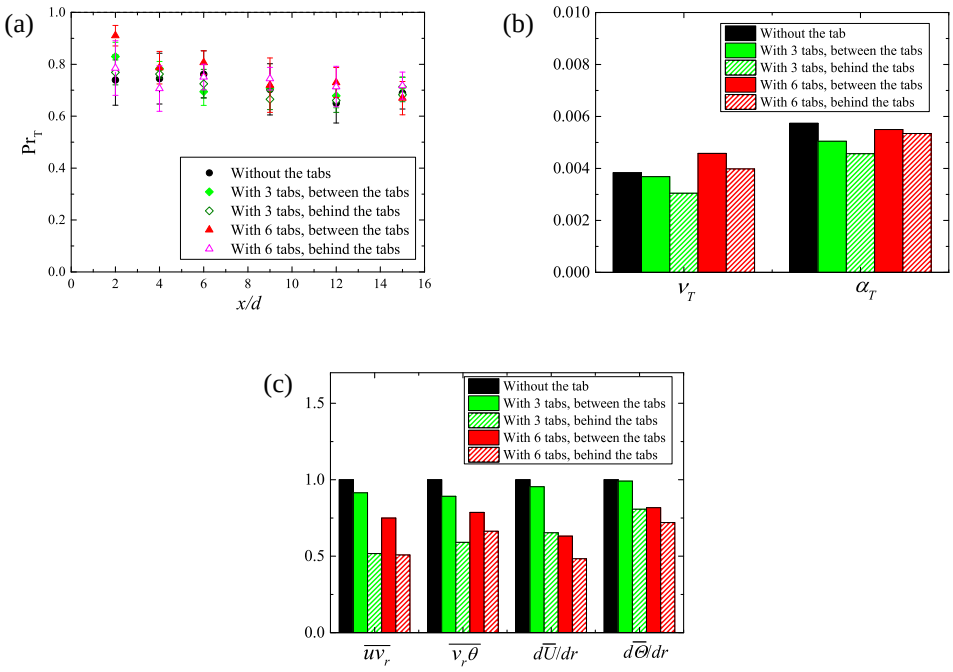

Figure 32: (a) Streamwise profiles of the turbulent Prandtl number at $\overline{U}/U_C = 0.5$; (b) eddy diffusivity coefficient ν_T and turbulent heat diffusivity coefficient α_T at $\overline{U}/U_C = 0.5$ and $x/d = 2$; (c) $\overline{uv_r}$, $\overline{v_r\theta}$, $d\overline{U}/dr$, and $d\overline{\Theta}/dr$ normalized by the values in the case without the tab.

cases without the tab and with 3 and 6 tabs. It illustrates that $\mathrm{Pr_T}$ is basically in the range of $0.6 \sim 0.8$ but it is larger in the upstream region at between the tabs. In particular, it is about 0.9 in the case with 6 tabs at $x/d = 2$. To clarify the reason of this, we show ν_T and α_T at $x/d = 2$ in Fig. 32(b) and the terms consisting them, $\overline{uv_r}$, $\overline{v_r\theta}$, $d\overline{U}/dr$, and $d\overline{\Theta}/dr$, normalized by the value in the case without the tab in Fig. 32(c). It turned out that $d\overline{U}/dr$ is relatively small at between the tabs in the case with 6 tabs. This phenomenon is also observed in the past studies [9, 19] and results in large ν_T, which consequently leads to large $\mathrm{Pr_T}$. Fig. 32(b) also shows that ν_T and α_T at behind the tabs are smaller than those at between the tabs. This reason can be explained by the vortical motion observed in Figs. 19(a) and 20(a). These figures illustrate that the jet spreads out from between the tabs and comes back toward the center from the area corresponding to behind the tabs. In other words, fluid mass with large velocity and high temperature recirculates at behind the tabs. Therefore, momentum and thermal diffusion behind the tabs is relatively

small in spite of the large velocity and temperature gradients.

4. Conclusions

In the present study, the effects of half-delta wing tabs in an axisymmetric jet are experimentally investigated. The number of the tab was varied from 1 to 6. The main conclusions are as follows. The mixing of the ambient fluid is more enhanced with increasing the number of the tab near the jet exit. However, in the downstream region, it is suppressed in the cases with 4, 5, and 6 tabs and most suppressed in the case with 6 tabs, while it is most enhanced in the case with 3 tabs. The analysis based on the mean velocity distribution indicates that, although the spatially-averaged entrainment velocity is basically decreased by the tabs, the mixing and entrainment can be enhanced when the entrainment area is significantly increased. The thermal diffusion also increases with increasing the number of the tab near the jet exit, but in the downstream region, it is equivalent or smaller in the case with the tabs. These results are caused by the mixed effects of the tabs: enhancement of not only mixing and diffusion but also the energy dissipation.

The present study suggests that it is feasible to both promote and suppress mixing of the jet by the half delta-wing tabs, and directional characteristics of the jet diffusion can be controlled by optimizing the tab installation.

Acknowledgement

Part of this study was supported by Hibi Kagaku Gijutu Zaidan. The authors express their gratitude to Prof. Koji Nagata (Nagoya University), Dr. Osamu Terashima (Toyama Prefectural University) and Mr. Mamoru Takahashi (Nagoya University) for their useful comments, and Mr. Kosuke Naganawa (Nagoya University) for his help for paper preparation.

References

[1] B. L. Smith, a. Glezer, Jet vectoring using synthetic jets, Journal of Fluid Mechanics 458 (2002) 1–34.

[2] N. Benard, J. P. Bonnet, G. Touchard, E. Moreau, Flow Control by Dielectric Barrier Discharge Actuators: Jet Mixing Enhancement, AIAA Journal 46 (2008) 2293–2305.

[3] H. Suzuki, N. Kasagi, Y. Suzuki, Active control of an axisymmetric jet with distributed electromagnetic flap actuators, Experiments in Fluids 36 (2004) 498–509.

[4] W. R. Quinn, Streamwise evolution of a square jet cross section, AIAA Journal 30 (1992) 2852–2857.

[5] E. K. Longmire, J. K. Eaton, C. J. Elkins, Control of jet structure by crown-shaped nozzles, AIAA Journal 30 (1992) 505–512.

[6] K. B. M. Q. Zaman, Spreading characteristics of compressible jets from nozzles of various geometries, Journal of Fluid Mechanics 383 (1999) 197–228.

[7] L. J. S. Bradbury, A. H. Khadem, The distortion of a jet by tabs, Journal of Fluid Mechanics 70 (1975) 801–813.

[8] K. B. M. Q. Zaman, M. F. Reeder, M. Samimy, Control of an axisymmetric jet using vortex generators, Physics of Fluids 6 (1994) 778–793.

[9] N. Heeb, E. Gutmark, K. Kailasanath, An experimental investigation of the flow dynamics of streamwise vortices of various strengths interacting with a supersonic jet, Physics of Fluids 26 (2014).

[10] K. Nagata, Y. Sakai, K. Hiromori, T. Kubo, Y. Oguro, Active control of an axisymmetric turbulent jet using moving prominences (effect of shapes and moving patterns of the prominences), Transaction of Japan Society of Mechanical Engineering, Series B 75 (2009) 1296–1303 (in Japanese).

[11] M. J. Carletti, C. B. Rogers, D. E. Parekh, Parametric study of jet mixing enhancement by vortex generators, tabs, and deflector plates, American Society of Mechanical Engineering, Fluids Engineering Division Conference 237 (1996) 303–312.

[12] C. B. Rogers, D. E. Parekh, Mixing enhancement by and noise characteristics of streamwise vortices in air jet, AIAA Journal 32 (1994) 464–471.

[13] J. Mi, G. Nathan, Effect of small vortex-generators on scalar mixing in the developing region of a turbulent jet, International Journal of Heat and Mass Transfer 42 (1999) 3919–3926.

[14] N. Heeb, E. Gutmark, K. Kailasanath, Impact of chevron spacing and asymmetric distribution on supersonic jet acoustics and flow, Journal of Sound and Vibration 370 (2016) 54–81.

[15] M. Hirota, H. Fujita, H. Yokosawa, Influences of velocity gradient on hot-wire anemometry with an X-wire probe, Journal of Physics E: Scientific Instruments 21 (1988) 1077–1084.

[16] M. Tagawa, K. Kato, Y. Ohta, Response compensation of fine-wire temperature sensors, Review of Scientific Instruments 76 (2005).

[17] H. H. Brunn, Hot-wire anemometry, Oxford University Press, 1975.

[18] T. Watanabe, Y. Sakai, K. Nagata, Y. Ito, T. Hayase, Turbulent mixing of passive scalar near turbulent and non-turbulent interface in mixing layers, Physics of Fluids 27 (2015).

[19] Y. Ito, K. Nagata, Y. Sakai, O. Terashima, Momentum and mass transfer in developing liquid shear mixing layers, Experimental Thermal and Fluid Science. 51 (2013) 28–36.

[20] R. Everson, D. Manin, L. Sirovich, M. Winter, Quantification of mixing and mixing rate from experimental observations, AIAA Journal 36 (1998) 121–127.